INTERNATIONAL JOURNAL OF ADVANCED RESEARCH
International Peer-Reviewed Research Journal
ISSN (Online): 3106-7980 | ISSN (Print): 3106-7972
Volume 3 • Issue 5 • September 2026

NUMERICAL SIMULATION OF AN ENVIRONMENTAL FRIENDLY PEROVSKITE ($CH_3NH_3SnBr_3$) BASED SOLAR CELL

Azmat Ali[*1,5], Summan Iqbal[1,5], Ahmed Salim[2], Su Rahman[3], Mohsin M. Tarar[4]

[*1]*Department of Physics, University of Chakwal, Chakwal, Pakistan*
[2]*Department of Electrical Engineering, NAMAL University Mianwali, Pakistan*
[3]*Department of Mathematics, University of Chakwal, Chakwal, Pakistan*
[4]*Department of Electronics Engineering, University of Chakwal, Chakwal, Pakistan*
[5]*Department of Physics, COMSATS University Islamabad, Pakistan*

[*1]azmat.chakwal@gmail.com, [2]summan.iqbal26@gmail.com, [3]ahmed.salim@namal.edu.pk, [4]shafiq.urrahman@uoc.edu.pk, [5]mohsin.tarar@uoc.edu.pk

DOI: https://doi.org/10.5281/zenodo.23075993

Keywords
Perovskite solar cell, Hole Transport Layer, Electron Transport Layer, Perovskite Absorber Layer, Jsc, Voc, FF, eta, Working Temperature

Article History
Received: 01 June 2026
Accepted: 23 August 2026
Published: 08 September 2026

Copyright @Author
Corresponding Author: * **Azmat Ali**

Abstract
The stability and toxicity issues, lead (Pb)-based perovskite solar cells face significant limitations. Under such circumstances, the development of efficient perovskite solar cells (PSC) may depend heavily on tin (Sn)-based organic-inorganic perovskite solar cells. An environmentally friendly, stable, and lead (Pb) free $CH_3NH_3SnBr_3$-based organic-inorganic n-i-p-shaped perovskite solar cell (PSC) with the use of all inorganic charge transport elements for optimal reliability is suggested here by a theoretical investigation(1). By examining elements such as charge transport materials and their interface defect density, absorber defect density, ETL, HTL, and absorber thickness, a high-rise performance PSC is attained at room temperature. According to the data obtained, $CH_3NH_3SnBr_3$ has the potential to be a significant absorbing perovskite in perovskite solar cell technology(2).

1. INTRODUCTION

People's curiosity in sustainable energy sources has risen due to climate change, as the world's energy consumption is increasing daily due to non-renewable energy sources. One of the most affordable and eco-friendly solutions available is solar energy(3). The first solar cell design was stated by A. Kojima et al. in 2009, even though perovskite materials have long been known. They used mesoporous TiO2 sheets in conjunction with nanocrystals of the organometallic halide perovskites $CH_3NH_3PbI_3$ and $CH_3NH_3PbBr_3$ as an electron transport medium. They showed that these materials exhibit strong optical absorption and efficiencies of up to 3.13 percent and 3.8 percent, respectively(4). A 2-3 nm nanocrystal perovskite cell was created in 2011 by J.-H. Im et al. Quantum dots are produced by spin coating metal halide and organic-inorganic halide solutions on the TiO_2 surface. At a wavelength of 530 nm (EQE), they attained 78.6 percent external quantum efficiency

using the AM 1.5G sun intensity spectrum. Additionally, using these solar cells triggered an optimal power conversion efficiency of 6.54 percent(5). Therefore, the Power Conversion Efficiency (PCE) of lead-based perovskites solar cells (PVSCs) elevated from 3.9 percent to more than 22.7 percent between 2009 and 2019. Without a doubt, solar cells predicated on metal halide perovskites having a formula ABX_3 where X is a halide anion, B is a lead or tin cation, and A is either an organic or inorganic cation that has completely transformed the development of photovoltaic technology. (4, 6-9). Owing to its more economical and manufacturing simplicity, Perovskite, a third-generation solar cell, has the capability to become the most advanced photovoltaic technology in the modern society(10-12). Lead is environmentally toxic despite its high efficiency (13). As a result, it's critical to guarantee stability while guaranteeing photovoltaic efficiency in addition to lowering environmental toxicity by eradicating Pb from the perovskite composition(14, 15). Consequently, lead is replaced with tin (Sn), which is a clear choice among the several methods investigated because of their comparable ionic radii and electronic topologies that might preserve the

2. Theoretical concept:

The FTO/ETL/Absorber/HTL/Au one-dimensional n.i.p planar heterojunction structure makes up the stimulated Perovskite Solar Cell (PSC). The Electron Transport Layer (ETL), Perovskite Active Layer (PAL), and Hole Transport Layer (HTL) are displayed separately in each of the three regions (n, i, and p) in Figure 1. This structure uses lead-free organic-inorganic $CH_3NH_3SnBr_3$ as PAL, inorganic n-ZnO, n-CdS, and n-TiO2 as ETL, and inorganic p-CuSCN, p-CuI, p-MoO_3, and p-NiO as HTL. A and B are two ions, and X is a halide in the symmetric ABX_3 perovskite structure. It is believed that atom arrangement in the three-dimensional (3D) structure are related to the reliability needed for a chemical charge neutralization process(20). Perovskite minerals seem to have a straightforward basic structure, yet their structural deformation characteristics vary greatly(21). As a result, researchers investigated a tin (Sn)-based perovskite solar cell as a substitute, in which tin is substituted for lead and the material structure is modified to look like $ASnX_3$. Tin-based perovskite solar cells have two main merits: they are lead-free and can aid in further optimising the bandgap of the active layer. Reducing the active layer's acceptor doping concentration can increase the productivity of tin-based solar cells. The electron/hole mobility and absorber layer defect density can be computed using the following equation (22).

$$N_t = \frac{1}{\tau \sigma V_{th}} \quad (1)$$

$$\mu = \frac{Dq}{KT} \quad (2)$$

$$D = \frac{l^2}{\tau} \quad (3)$$

N_t is the defect density, τ is the charge carrier lifetime, μ is the electron and hole mobility, σ is the hole/electron capture cross section, V_{th} is the hole/electron thermal velocity, D is the diffusion coefficient, and l is the diffusion length. The following expression can also be used to compute

remarkable semiconducting capabilities of $APbX_3$(16). Using an organic-inorganic Perovskite Solar Cell (PSC) and a solar cell capacitance simulator (SCAPS 1D), the lead (Pb) free absorber used in this study is $CH_3NH_3SnBr_3$(17). Since organic charge transport materials exhibit hostile behavior with perovskite material because they are hygroscopic and costly, inorganic charge transport materials will be assessed. Because inorganic charge transfer materials offer clarity in the visible, ultraviolet, and infrared spectrum, researchers are taking these disadvantages into consideration. To achieve optimal performance, the best Hole Transport Layer (HTL) and Electron Transport Layer (ETL) for $CH_3NH_3SnBr_3$ based PSC will be selected by varying its thickness(18). Examine the absorber defect density, interface defect density, and how the device's operation is affected by working temperature. Power Conversion Efficiency (PCE), Fill Factor (FF), Open Circuit Voltage (Voc), and Short Circuit Current Density (Jsc) are performance metrics. Therefore, analysing the device performance using these criteria could help design environmentally benign Sn-based perovskite solar cells for cutting-edge advancements(19).

the effective valence band density of states Nv and the effective conduction band density of states Nc.

$$N_c = 2\left(\frac{2\pi m_n KT}{h^2}\right)^{\frac{3}{2}} \quad (4)$$

$$N_v = 2\left(\frac{2\pi m_p KT}{h^2}\right)^{\frac{3}{2}} \quad (5)$$

where m_p and m_n stand for the electron and hole, respectively. In this context, the diffusion length and electron and hole carrier lifetime values are obtained from the literature(23). Au and FTO have work functions of 5.1eV and 4.4eV, respectively. Therefore, the following equation can be employed to analyze the absorption coefficient.

$$\alpha = A_\alpha (h\vartheta . E_g)^{\frac{1}{2}} \quad (6)$$

For incoming radiation, a conventional AM1.5 G illumination spectrum (1000 Watt/m2; T = 300 K) was utilized. Therefore, the conventional layer thickness was utilised from many documented journal (21, 24, 25).

A Gaussian energy distribution with a characteristic energy of 0.1 eV was employed for all defect states during simulation, and the thermal velocity of the holes and electrons was found to be $1x10^7$.

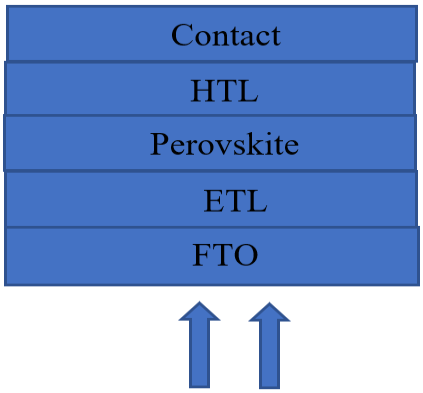


Figure 1: Layer-by-layer schematic of a regular-structured n-i-p perovskite photovoltaic device

3. Device structure and parameters:

A powerful tool for quickly understanding the physical behaviour of many optoelectronic characteristics of any solar cell is the simulation environment. The short circuit current density (Jsc), open circuit voltage (Voc), fill factor (FF), and efficiency (eta) of perovskite solar cells were explored in this study using the Solar Cell Capacitance Simulator (SCAPS 1-D)(26). The efficiency of a tin (Sn) based lead (Pb) free perovskite material that functions as an absorber layer and is positioned between the two transport layers was demonstrated through simulation-based theoretical study. Figure 1 depicts the device's configuration with ETL and HTL as FTO/ETL/$CH_3NH_3SnBr_3$/HTL/Au. In this case, Au and FTO have work functions of 5.1 eV and 4.4 eV, respectively.

4. Results and discussion:

This work uses self-developed codes to alter the thickness of the Perovskite Absorber Layer (PAL), Electron Transport Layer (ETL), and Hole Transport Layer (HTL). In addition, we suggest a novel structure to maximize PAL defect density, interface defects, and its operating temperature influence.

Table 1: Input parameters for different ETMs, HTMs with $CH_3NH_3SnBr_3$ of the PSC structure

	p-CuSCN	p-CuI	p-NiO	p-MoO_3	$CH_3NH_3SnBr_3$	n-TiO_2	n-ZnO	n-CdS
d (nm)	10	10	10	10	100	10	10	10

E_g (eV)	3.6	3.1	3.8	3	1.3	3.2	3.3	2.4
X (eV)	1.7	2.1	1.46	2.5	4.17	4.1	4.1	4.18
ε_r	10	6.5	10.7	12.5	10	9	9	10
N_c (cm^{-3})	2.2E+19	2.8E+19	2.8E+19	2.2E+18	2.2E+18	2.2E+18	2.2E+18	2.2E+18
$N_{v(}$ cm^{-3})	1.8E+18	1E+19	1E+19	1.8E+19	1.8E+18	1E+19	1.9E+19	1.9E+19
µn (cm^2/Vs)	100	100	12	25	1.6	20	100	100
µn (cm^2/Vs)	25	43.9	2.8	100	1.6	10	25	25
N_D (cm^{-3})	0	0	0	0	1E+13	1E+18	1E+18	1E+18
N_A (cm^{-3})	1E+18	1E+18	1E+18	1E+18	1E+13	0	0	0
N_t (cm^{-3})	1E+15	1E+15	1E+15	1E+15	1E+14	1E+15	1E+15	1E+15
Capture cross-section electrons (cm^2)	1E-15	1E-15	1E-15	1E-15	1E-15	2E-14	2E-14	2E-14
Capture cross-section holes (cm^2)	1E-15	1E-15	1E-15	1E-15	1E-15	2E-14	2E-14	2E-14

5.HTL optimization

To select the finest HTM and determine its ideal thickness, HTL is adjusted in this paper utilising inorganic hole transport materials such as MoO_3, CuI, NiO, and CuSCN. Table 1 provides the input parameters for various HTMs. The SCAPS program uses all these parameters to optimise various HTMs by adjusting their thickness. Here, Table 2 displays the device performance for various HTMs, and Fig. 2 displays the matching J-V characteristics for all the HTMs used in this work. Therefore, it is obvious from Table 2 and Fig. 2 that MoO3 has the best j-v properties, better PCE, and better Voc of all HTMs. MoO3 exhibits the best band alignment with $CH_3NH_3SnBr_3$ because it has a higher PCE than other HTMs. Most preferably the structure or device with highest or which possess best PCE will be chosen and then the thickness is varied to optimize it.

INTERNATIONAL JOURNAL OF ADVANCED RESEARCH
International Peer-Reviewed Research Journal
ISSN (Online): 3106-7980 | ISSN (Print): 3106-7972
Volume 3 • Issue 5 • September 2026

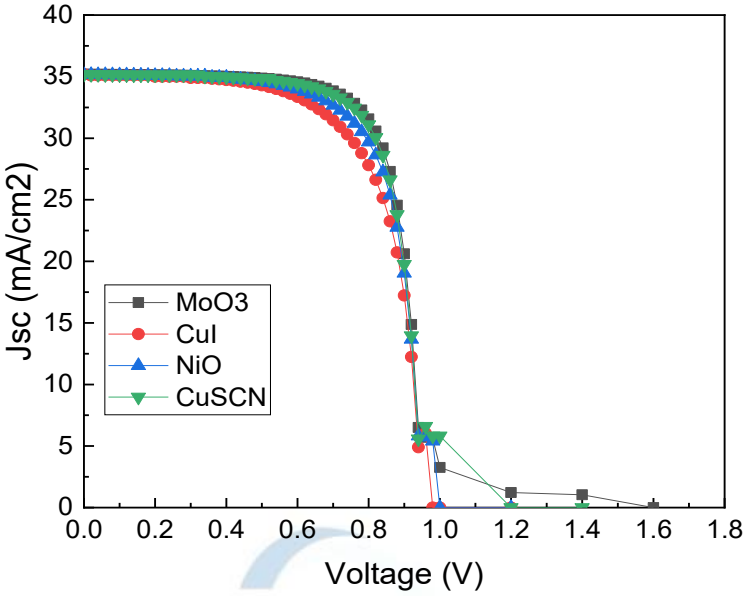


Table 2: Performance parameters of different HTMs as HTL.

Hole Transport Material	J_{sc} (mA/cm^2)	V_{oc} (V)	FF (%)	PCE (%)
NiO	35.341772	0.950358	70.9215	23.8207
CuI	35.323706	0.949952	67.0406	22.496
CuSCN	35.355784	0.949283	74.2183	24.9096
MoO_3	35.367187	0.950754	75.1763	25.2784

Fig.2. Comparative J-V Analysis of Diverse Hole Transporting Materials

As Table 2 shows the different HTMs parameters result, which shows that MoO_3 owns the best PCE and hence MoO_3 is chosen to optimize its thickness. The regular practicability of the manufacturing technique of perovskite solar cells should be kept in mind, the thickness of HTL should be varied from 10nm to 200nm to optimize it (27). Hence to further clarify Fig. 3 shows the result of all parameters of HTL by varying its thickness, it comprises of all HTMs as shown below and hence from all these HTMs one will be showing higher efficiency as compared to others or will be showing best performance than other HTMs. So, the main task is to select that HTM which shows more efficiency than all other HTMs and hence optimized. MoO_3 shows the best results as shown in Fig. 3. Consequently, MoO_3 is chosen as HTL for this device and Fig. 4 shows the optimization curve of HTL by varying the thickness for MoO_3 and optimizing it. All four parameters J_{sc}, V_{oc}, FF and PCE are drawn in a single frame to make it easy to understand that at which thickness it will be more efficient.

INTERNATIONAL JOURNAL OF ADVANCED RESEARCH
International Peer-Reviewed Research Journal
ISSN (Online): 3106-7980 | ISSN (Print): 3106-7972
Volume 3 • Issue 5 • September 2026

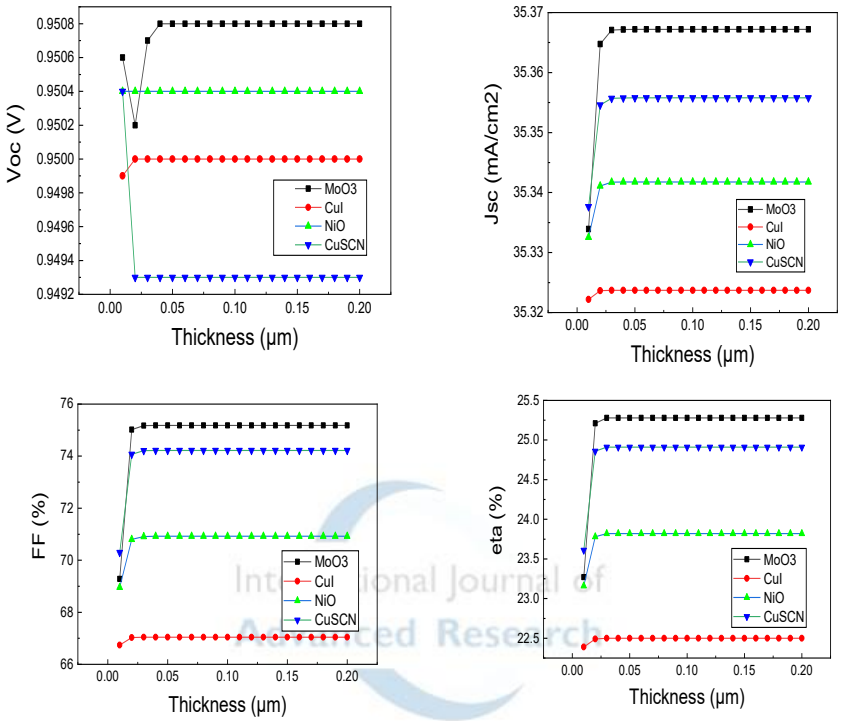


Fig. 3. PCE, FF, Voc and Jsc curve against all HTLs.

In Fig. 4, at first Voc decreases abruptly when thickness of HTL increases but then as thickness of HTL is further increased so it shows a gradual increase in it. The FF, Jsc and PCE initially increases and then almost get equal to constant when the thickness of HTL further increases. It may happen due to current leakage and low shunt resistance at small thickness and the rising series resistance with the rise in HTM thickness (28). The Perovskite Structure with MoO_3 as HTM shows the supreme result at 40nm having Voc = 0.9508 V, Jsc = 35.36718 mA/cm^2, FF = 75.18 %, PCE = 25.28%. Therefore, MoO_3 is selected as an optimum HTM for $CH_3NH_3SnBr_3$ perovskite structure with an optimized thickness of 40nm.(29)

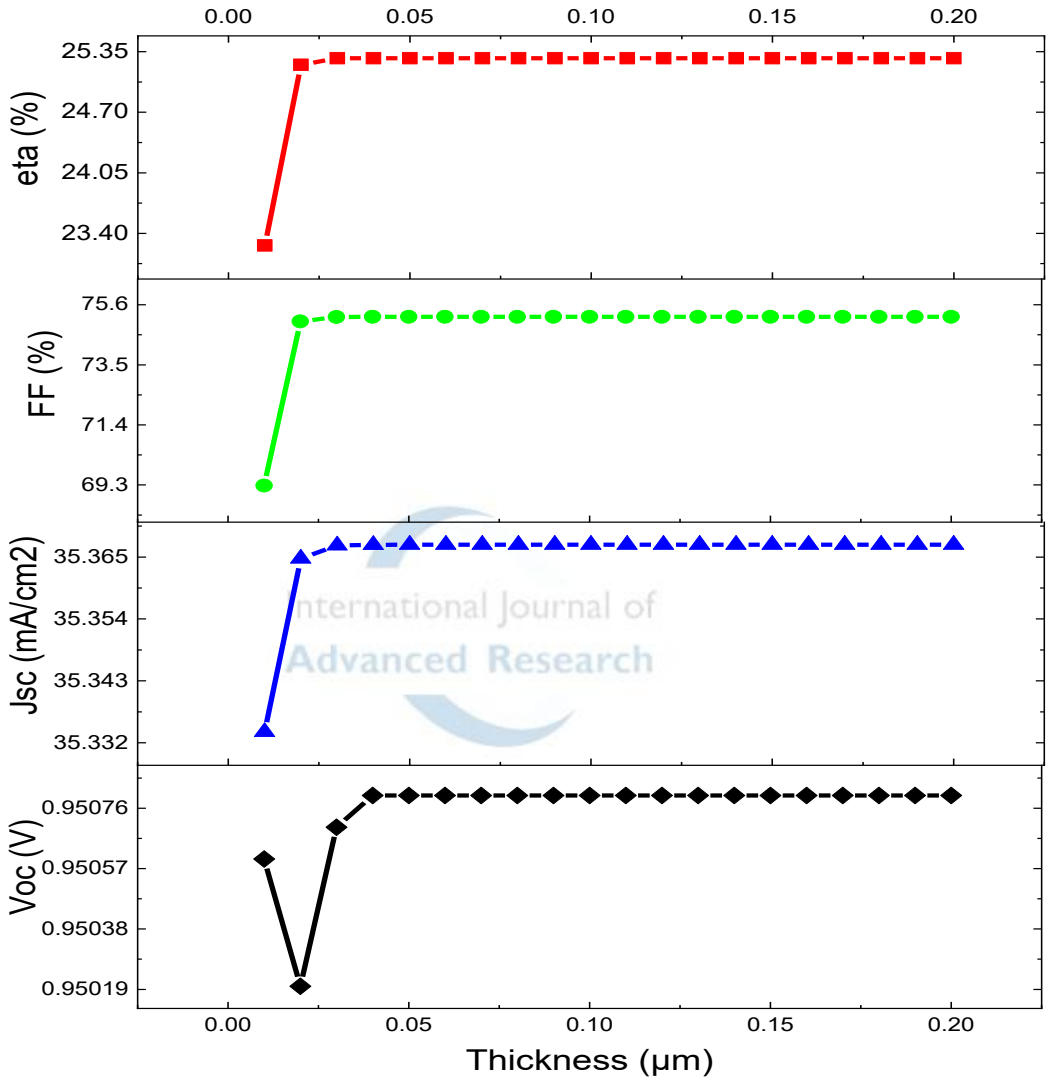


Fig. 4. HTL optimization curve by varying the thickness for MoO_3 as HTM.

INTERNATIONAL JOURNAL OF ADVANCED RESEARCH
International Peer-Reviewed Research Journal
ISSN (Online): 3106-7980 | ISSN (Print): 3106-7972
Volume 3 • Issue 5 • September 2026

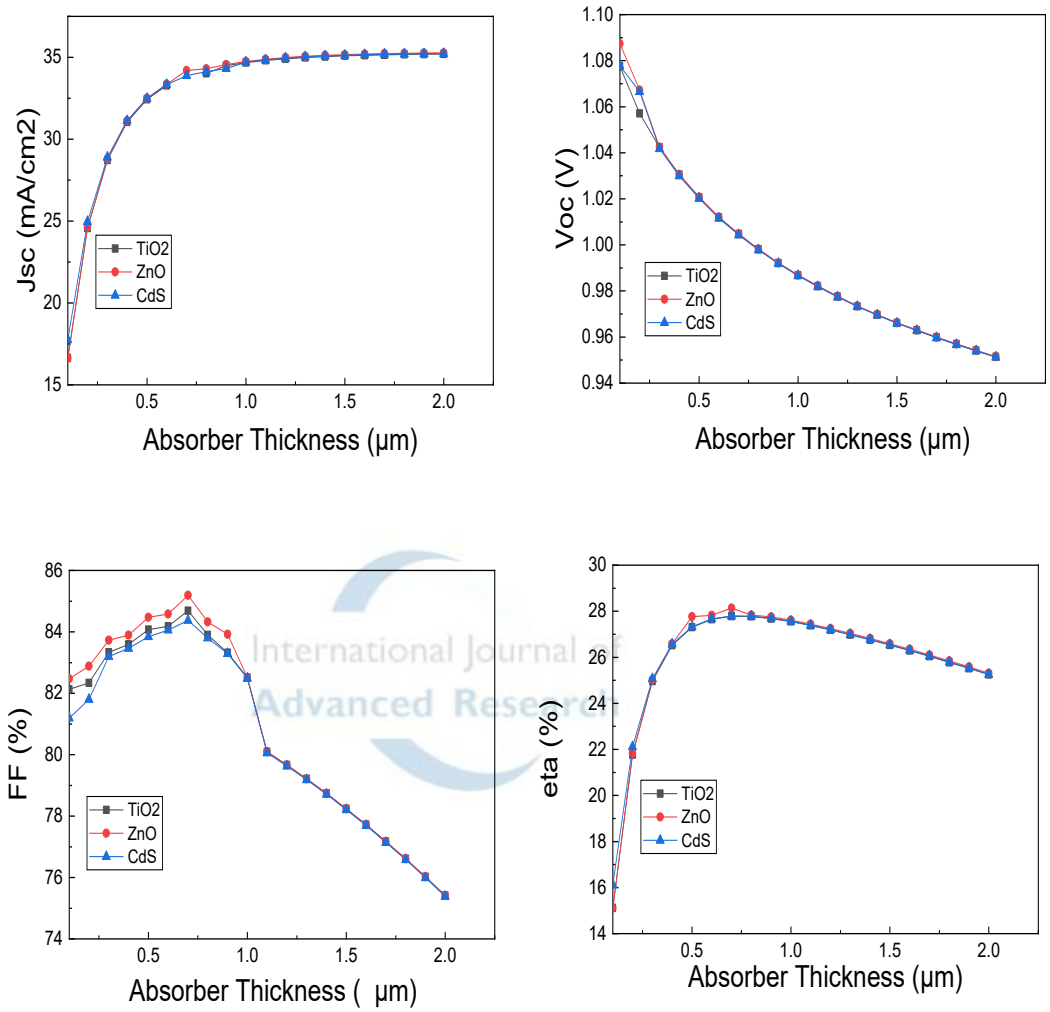


Fig. 5. Jsc, Voc, FF, and PCE curves as a function of absorber thickness for CH3NH3SnBr3 with different ETMs.

The optimization of the absorber thickness $CH_3NH_3SnBr_3$ occurs by using different ETMs as displayed in fig. 5. Here the thickness of the absorber spans from 100-2000nm for every ETM which is used in this technique that are Cds, TiO_2 and ZnO.

From fig 5, it's obvious that ZnO provides finest findings than other ETMs. While increasing the absorber thickness, PCE, FF and Jsc initially rise up to 700nm thickness hence then Jsc almost get equal to constant, however PCE and FF starts decreasing when thickness is further increased from 700nm to 2000nm and V_{oc} decreases when thickness of absorber is varied(30, 31), as depicted in fig. 5.

Consequently, from Fig 5 ZnO displays the optimal results than other ETMs, when the thickness of absorber is 100-700nm so PCE, FF and Jsc increases and reaches to 28.14%, 85.19% and 34.20 mA/cm^2 but from 700nm-2000nm Jsc almost get equal to constant whereas PCE and FF shows a gradual decrease for ZnO. However, in case of Voc there is no such change as it decreases when the thickness is varied. So, at 700nm ZnO shows the best PCE value of 28.14% than other ETMs. All the ETMs shows a good band alignment with absorber due to which a constant Jsc is obtained (32), when thickness is varied more and more. As the obtained value of FF and Jsc at 700nm for TiO_2 are 84.69%

and 33.84mA/cm^2, for CdS are 84.37%, 33.88mA/cm^2 and for ZnO are 85.19%, 34.20mA/cm^2 due to the alteration into their Quantum efficiency (QE) as illustrated in fig6.

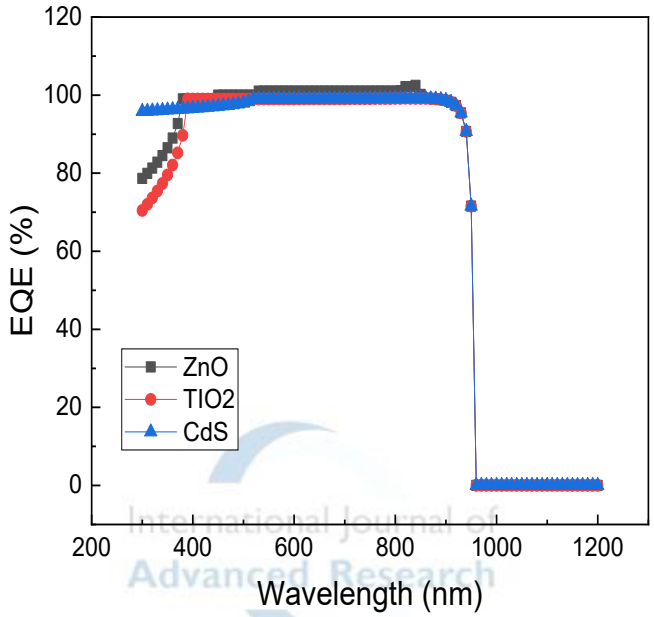


Fig 6. Quantum efficiency curve at the optimized absorber thickness of different ETMs.

From Fig. 6, it's obvious that ZnO show larger QE than all other ETMs in the visible range. Hence ZnO hold best Jsc, FF and PCE by comparing to other ETMs used in this perovskite solar cell (PSC) so therefore the optimized perovskite active layer thickness will be 700nm for ZnO, as at this thickness it shows the best result for Perovskite active layer (PAL)(33).

6. ETL thickness optimization

ZnO is selected as an ETL and should be optimised by altering its thickness from 10 nm to 200 nm because it exhibits the best PCE and FF when perovskite active layer (PAL) is optimised. The optimized thickness of both HTL and PAL should be utilised and maintained until ETL is also optimised. Thus, Jsc, Voc, FF, and PCE are plotted versus ETL thickness variation in Fig. 7. Thus, the optimal ETL thickness at 10 nm has the maximum Jsc (35.36366 mA/cm^2), Voc (0.9517 V), FF (75.41%), and PCE (25.38%). Thus, all the optimised HTL, ETL, and PAL produced high yield PSC using a unique combination of FTO/ZnO/$CH_3NH_3SnBr_3$/MoO_3/Au. The innovative structure's diagrammatic representation is displayed in Fig. 8. This unique combination demonstrates that all three HTL, ETL, and PAL become optimised at a particular thickness. As a result, all three layers for the optimised device are depicted in Figure 8.(33, 34)

INTERNATIONAL JOURNAL OF ADVANCED RESEARCH
International Peer-Reviewed Research Journal
ISSN (Online): 3106-7980 | ISSN (Print): 3106-7972
Volume 3 • Issue 5 • September 2026

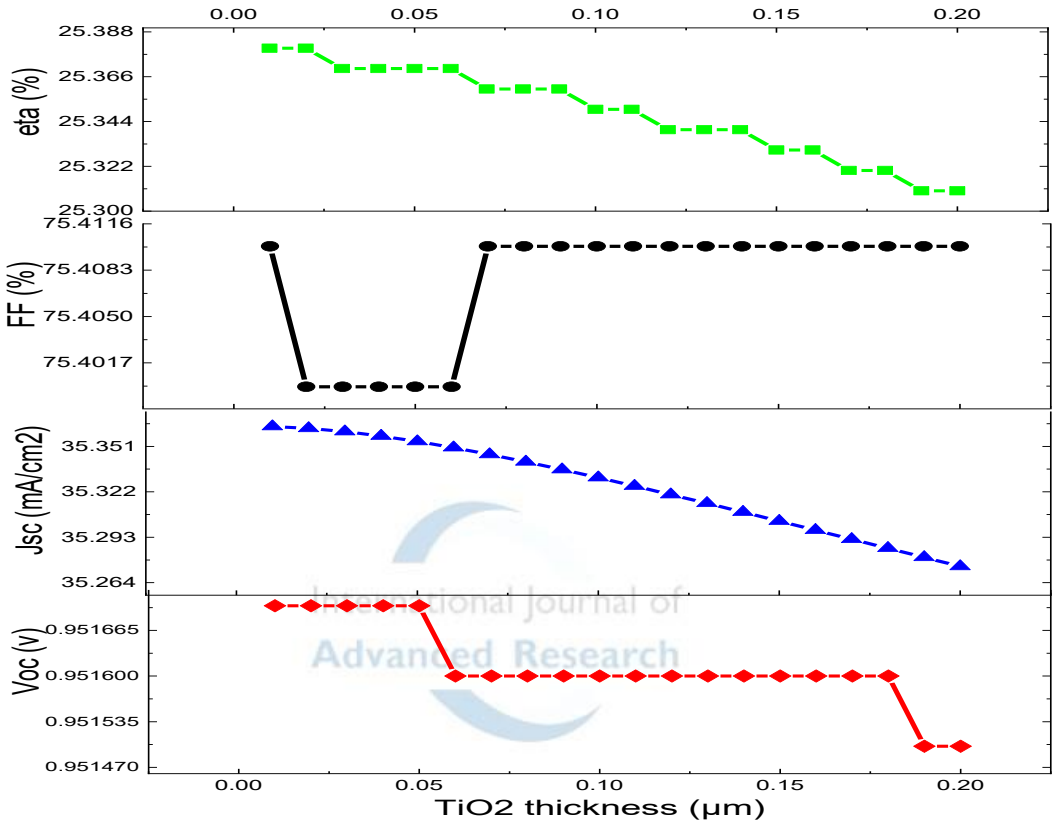


Fig. 7. Thickness variation of ETL shows change in PCE, FF, Voc and Jsc.

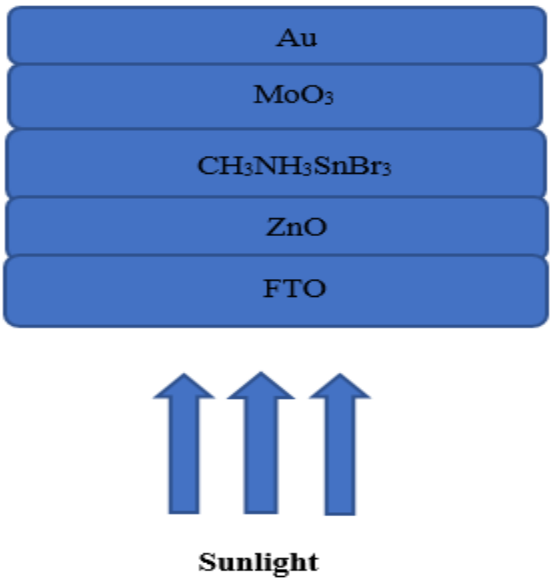


Fig. 8. Simplified diagram of the optimized device FTO/ZnO/$CH_3NH_3SnBr_3$/MoO_3/Au.

1. Absorber defect density optimization

Therefore, utilising specific HTM, ETM, and optimised thickness of HTL, ETL, and PAL, the defect density is altered from 10^{12} cm^{-3} to 10^{19} cm^{-3} to investigate its impact. The J-V characteristics curve at several defect densities can now be depicted in Fig. 9. When the defect density exceeds 10^{15} cm^{-3}, the Jsc of PSC collapses from 33.87 mA/cm^2 at 10^{15} cm^{-3} to 0.03885 mA/cm^2 at 10^{19} cm^{-3}. This collapse is actually caused by an increase in the recombination rate with rising defect density(35). However, when the defect density is less than 10^{15} cm^{-3}, it essentially stays unaffected. Consequently, an optimised defect density of 10^{15} cm^{-3} was achieved, along with Voc of 0.898 V, Jsc of 33.87 mA/cm^2, FF of 79.23%, and PCE of 24.13%.

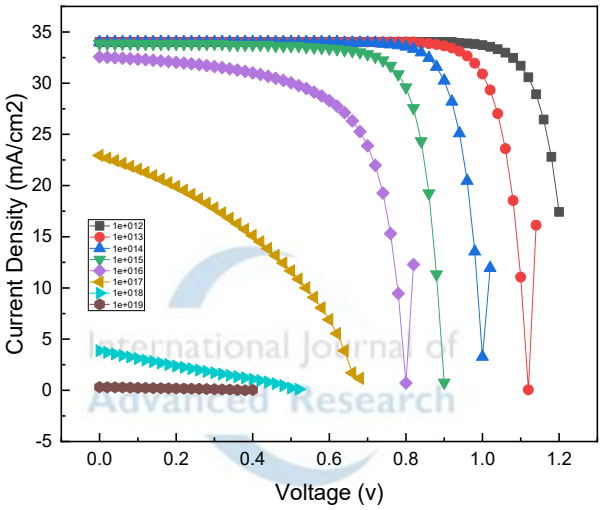


Fig. 9. J-V curve for different absorber defect density.

2. Interface defect density optimization

The absorber/ETL and HTL/absorber interface defect densities are analysed for values between 10^6 and 10^{13} cm^{-3}. The J-V characteristics for both interface fault densities are thus displayed in Fig. 10. Therefore, it is clear from Fig. 10 that the parameters change infinitesimally below 109 cm^{-3} before Jsc saturates. Nevertheless, Jsc drops from 34.01 mA/cm^2 to 30.01 mA/cm^2 above 109 cm^{-3} to 1013 cm^{-3}. Reduction actually happens as a result of the interface defect that creates more traps at recombination centers(31). Consequently, Jsc is 34.01 mA/cm^2, Voc is 1.05 V, FF is 81.69%, and PCE is 27.91% at the optimised interface defect of 109 cm^{-3}.

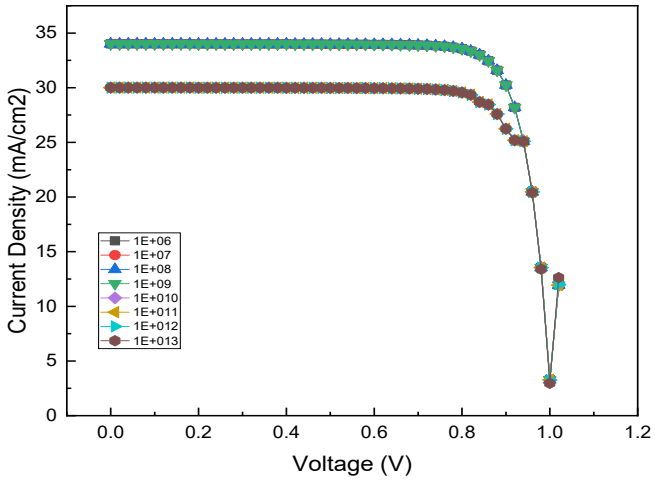


Fig. 10. comparison of J-V graph for different interface defects.

3. Optimized device

As seen above in Fig. 8, the device is optimised with all ETL, HTL, and PAL by obtaining high efficiency PSC with a new combination. Thus, Figs. 11 and 12 display the QE curve and J-V characteristics curve for the optimised device. Near 380 nm, which is in the visible range, the device provides Jsc of 34.01 mA/cm^2, Voc of 1.05 V, FF of 81.69%, PCE of 27.91%, and 99.98% QE. As previously stated, SCAPS-1D is used to determine all of these factors.(26).

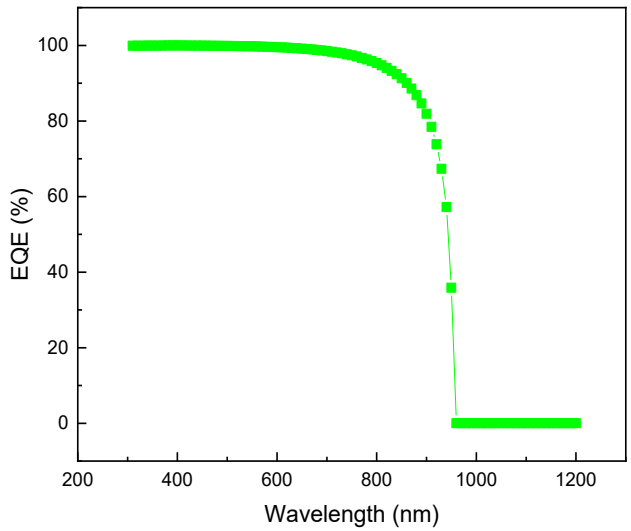


Fig.11. Optimized FTO/ZnO/$CH_3NH_3SnBr_3$/MoO_3/Au structure EQE curve.

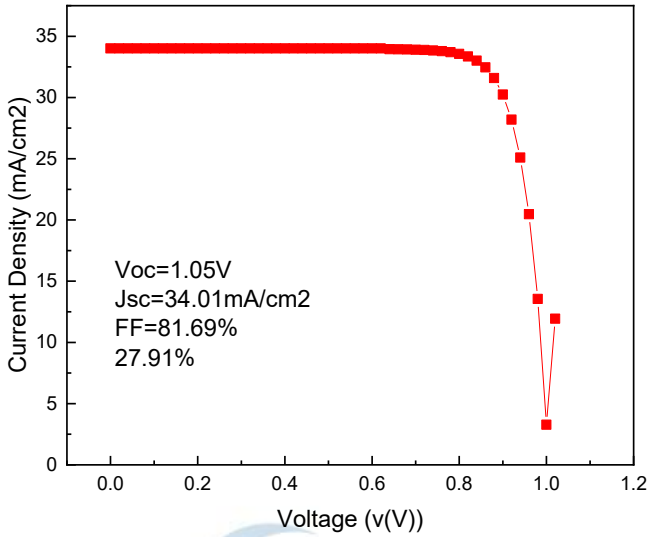


Fig. 12. J-V characteristics curve for the optimized device

Both graphs show that this device yields quite promising results, is environmentally benign, and is expected to be more stable in nature because it is composed solely of inorganic transport components. The device's dark J-V characteristics curve is illustrated in Fig. 13.

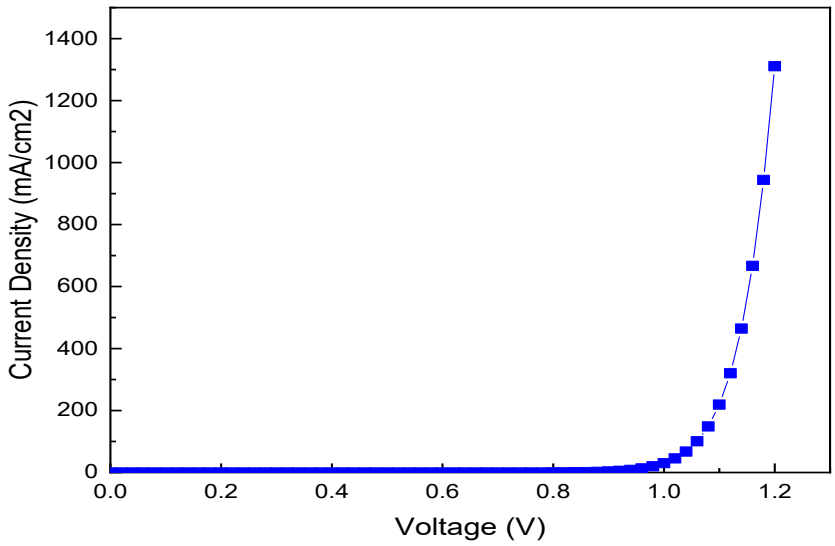


Fig.13. Dark J-V characteristics curve for optimized FTO/ZnO/$CH_3NH_3SnBr_3$/MoO_3/Au structure.

INTERNATIONAL JOURNAL OF ADVANCED RESEARCH
International Peer-Reviewed Research Journal
ISSN (Online): 3106-7980 | ISSN (Print): 3106-7972
Volume 3 • Issue 5 • September 2026

4. Working temperature effect

One must examine the device's performance for a range of operating temperatures, from 260 K to 400 K, to acquire a clearer understanding of how the device behaves in the natural world. Therefore, Fig. 14 illustrates that a deterioration happens when the working temperature is increased between 260 and 400 K. When the temperature rises, all four parameters gradually decline: Voc drops from 1.05 V to 0.87 V, Jsc from 34.009 mA/cm^2 to 34.005 mA/cm^2, FF from 82.76% to 75.76%, and PCE from 30.07% to 22.37%. Thus, it results from thermal carrier creation and bandgap decrease(36).

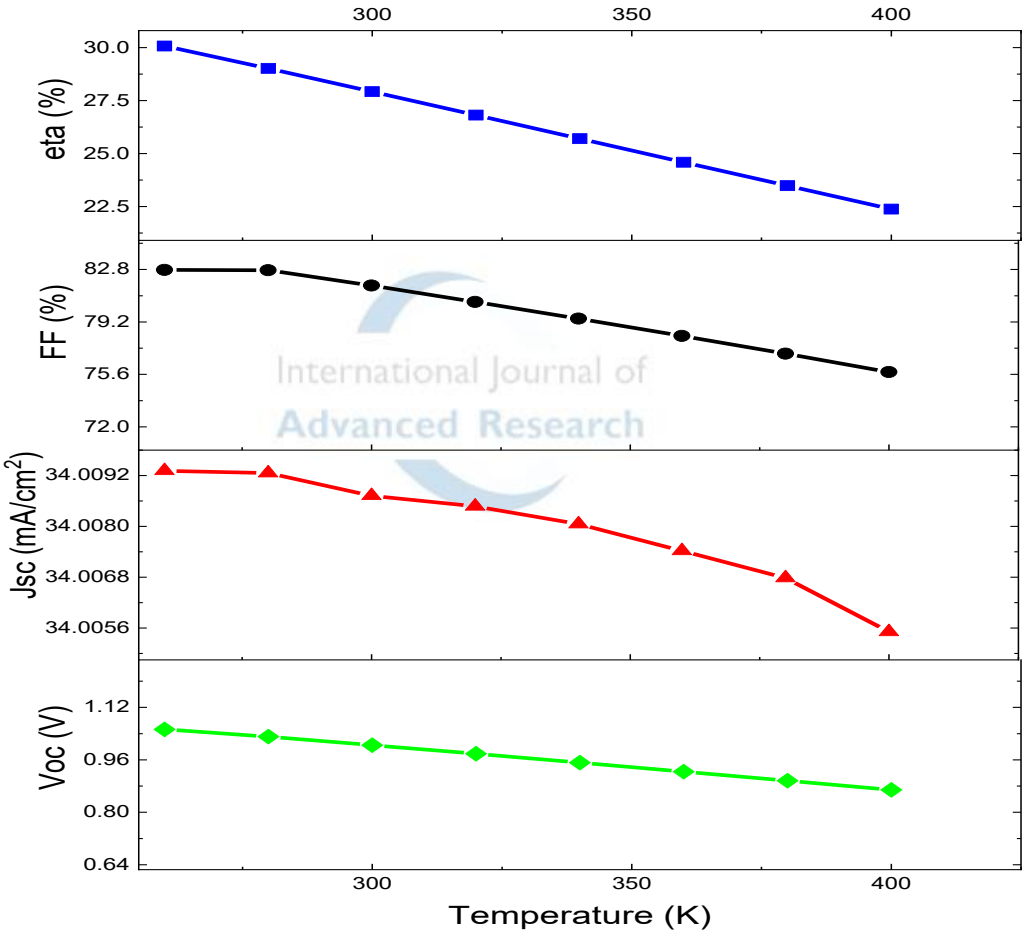


Fig.14. Temperature effect on Voc, Jsc, FF and eta.

Conclusion

This paper proposes an organic-inorganic perovskite solar cell (PSC) built upon $CH_3NH_3SnBr_3$ that is stable, lead-free, and environmentally benign using only inorganic charge transfer elements. One of the supreme materials is selected in each scenario after analysing the effects of various ETL and HTL materials, and the layer thickness is then optimised. The combination of FTO/ZnO/ $CH_3NH_3SnBr_3$ /MoO_3 /Au is then proposed as a high yield n-i-p solar cell. Near 380 nm, which is near the Uv visible boundary, the developed device runs at a high level of efficiency (PCE) of 27.91%, short circuit current density (Jsc) of 34.01 mA/cm^2, open circuit voltage (Voc) of 1.05 V, fill factor (FF) of 81.69%, and

quantum efficiency (QE) of 99.98%. This research paradigm is somewhat comparable to other studies and could be beneficial in creating lead-free, sustainable Sn based PSCs for upcoming technologies(37).

REFERENCES:

1. Yang J, Zhu G, Zheng Q, Liu Y, Dong H, Liu Y, et al. Performance improvement of low-dimensional Sn-based perovskites for solar cells from photophysical response to inter-phase transport and stability. Communications Materials. 2026;7(1):148.
2. Huang C, Huang Y, Zhao Q, Liu Z, Shen G, Jiang Q, et al. Eco-friendly lead-free and low-lead perovskite solar cells. Energy Materials and Devices. 2026;4(1):9370089.
3. Fraunhofer IJP-RpGtria. Photovoltaics Report https://ise. fraunhofer. de/content/dam/ise/de/documents/publications/studies. 2020.
4. Kojima A, Teshima K, Shirai Y, Miyasaka TJJotacs. Organometal halide perovskites as visible-light sensitizers for photovoltaic cells. 2009;131(17):6050-1.
5. Im J-H, Lee C-R, Lee J-W, Park S-W, Park N-GJN. 6.5% efficient perovskite quantum-dot-sensitized solar cell. 2011;3(10):4088-93.
6. Burschka J, Pellet N, Moon S-J, Humphry-Baker R, Gao P, Nazeeruddin MK, et al. Sequential deposition as a route to high-performance perovskite-sensitized solar cells. 2013;499(7458):316-9.
7. Green MA, Ho-Baillie A, Snaith HJJNp. The emergence of perovskite solar cells. 2014;8(7):506-14.
8. Shin SS, Yeom EJ, Yang WS, Hur S, Kim MG, Im J, et al. Colloidally prepared La-doped BaSnO3 electrodes for efficient, photostable perovskite solar cells. 2017;356(6334):167-71.
9. Yang WS, Park B-W, Jung EH, Jeon NJ, Kim YC, Lee DU, et al. Iodide management in formamidinium-lead-halide–based perovskite layers for efficient solar cells. 2017;356(6345):1376-9.
10. Gao P, Grätzel M, Nazeeruddin MKJE, Science E. Organohalide lead perovskites for photovoltaic applications. 2014;7(8):2448-63.
11. Singh V, Grover N, Agarwal PB, Arora P. Multiphysics Modeling and Optimization of High-Efficiency Lead-Free CH3NH3SnBr3 Perovskite Solar Cells. Advanced Theory and Simulations. 2026;9(4):e70399.
12. Thakur A, Raj M, Deupa M, Surapaneni R, Gupta S, Goel N. Review and perspectives of perovskite solar cells: toward environmentally sustainable and efficient photovoltaics. Energy & Fuels. 2025;39(51):24012-44.
13. Giustino F, Snaith HJJAEL. Toward lead-free perovskite solar cells. 2016;1(6):1233-40.
14. Sharma A, Srivastava AK, editors. A Study on Thickness Optimization and Variation in Lead Free Perovskite $\text {CH} _ {3}\text {NH} _ {3}\text {SnBr} _ {3} $. 2025 10th International Conference on Signal Processing and Communication (ICSC); 2025: IEEE.
15. Shafi MA, Ullah H, Ullah S, Khan L, Bibi S, Soucase BM. Numerical simulation of lead-free Sn-based perovskite solar cell by using SCAPS-1D. Engineering Proceedings. 2022;12(1):92.
16. Liu X, Yang Z, Chueh C-C, Rajagopal A, Williams ST, Sun Y, et al. Improved efficiency and stability of Pb–Sn binary perovskite solar cells by Cs substitution. 2016;4(46):17939-45.
17. Samiul Islam M, Sobayel K, Al-Kahtani A, Islam M, Muhammad G, Amin N, et al. Defect study and modelling of SnX3-based perovskite solar cells with SCAPS-1D. Nanomaterials. 2021;11(5):1218.
18. Aslam MHR. Optimization of ETL layers for CH3NH3SnBr3-perovskite solar cells through numerical analysis. Materials Today Communications. 2025:114279.
19. Jamalvandi B, Oftadeh M. Chemical Methodologies. 2021.

20. Park N-GJMt. Perovskite solar cells: an emerging photovoltaic technology. 2015;18(2):65-72.
21. Islam S, Sobayel K, Al-Kahtani A, Islam M, Muhammad G, Amin N, et al. Defect study and modelling of SnX3-based perovskite solar cells with SCAPS-1D. 2021;11(5):1218.
22. Du H-J, Wang W-C, Zhu J-ZJCPB. Device simulation of lead-free CH3NH3SnI3 perovskite solar cells with high efficiency. 2016;25(10):108802.
23. Chen M, Ju M-G, Carl AD, Zong Y, Grimm RL, Gu J, et al. Cesium titanium (IV) bromide thin films based stable lead-free perovskite solar cells. 2018;2(3):558-70.
24. Baktash A, Amiri O, Sasani AJS, Microstructures. Improve efficiency of perovskite solar cells by using magnesium doped ZnO and TiO2 compact layers. 2016;93:128-37.
25. Liu F, Zhu J, Wei J, Li Y, Lv M, Yang S, et al. Numerical simulation: toward the design of high-efficiency planar perovskite solar cells. 2014;104(25):253508.
26. Kang AK, Zandi MH, Gorji NEJO, Electronics Q. Simulation analysis of graphene contacted perovskite solar cells using SCAPS-1D. 2019;51(4):1-9.
27. Shahiduzzaman M, Yamamoto K, Furumoto Y, Kuwabara T, Takahashi K, Taima TJCL. Enhanced photovoltaic performance of perovskite solar cells via modification of surface characteristics using a fullerene interlayer. 2015;44(12):1735-7.
28. Lin L, Jiang L, Li P, Qiu Y, Yan QJJoPfE. Numerical analysis of inverted-structure perovskite solar cell based on all-inorganic charge transport layers. 2019;9(2):024501.
29. Schulz P, Tiepelt JO, Christians JA, Levine I, Edri E, Sanehira EM, et al. High-work-function molybdenum oxide hole extraction contacts in hybrid organic–inorganic perovskite solar cells. ACS applied materials & interfaces. 2016;8(46):31491-9.
30. Aliaghayee M. An overview of the numerical modeling, simulation, and optimization methods: toward the design of highly efficient planer perovskite solar cells. Discover Electronics. 2024;1(1):35.
31. Abdelaziz W, Shaker A, Abouelatta M, Zekry AJOM. Possible efficiency boosting of non-fullerene acceptor solar cell using device simulation. 2019;91:239-45.
32. Minemoto T, Murata MJSEM, Cells S. Theoretical analysis on effect of band offsets in perovskite solar cells. 2015;133:8-14.
33. Zhang P, Wu J, Zhang T, Wang Y, Liu D, Chen H, et al. Perovskite solar cells with ZnO electron-transporting materials. Advanced Materials. 2018;30(3):1703737.
34. Zainal Abidin NA, Arith F, Noorasid NS, Sarkawi H, Mustafa AN, Safie N, et al. Dopant engineering for ZnO electron transport layer towards efficient perovskite solar cells. RSC advances. 2023;13(48):33797-819.
35. Salah MM, Abouelatta M, Shaker A, Hassan KM, Saeed AJSS, Technology. A comprehensive simulation study of hybrid halide perovskite solar cell with copper oxide as HTM. 2019;34(11):115009.
36. Green MAJEC. Solar cells: operating principles, technology, and system applications. 1982.
37. Sarker MS, Piya MI, Fahim SR, Hasan MK, Mamur H, Bhuiyan MRA. Optimizing the performance of CH3NH3SnBr3–based PSCs with SCAPS-1D and machine learning techniques. Chemistry of Inorganic Materials. 2026:100153.

International Journal of Advanced Research